Title

Kinetics of n-Hexane Cracking over ZSM-5 Zeolites

-Effect of Crystal Size on Effectiveness Factor and Catalyst Lifetime-

Authors

Hiroki Konno, Takuya Okamura, Takahito Kawahara,

Yuta Nakasaka, Teruoki Tago* and Takao Masuda

Division of Chemical Process Engineering, Faculty of Engineering,

Hokkaido University, N13 W8, Kita-ku, Sapporo, Hokkaido 060-8628, Japan

** Corresponding author:*

E-mail: tago@eng.hokudai.ac.jp

Tel:+81-117066551

Fax: +81-117066552

Abstract

The catalytic cracking of *n*-hexane over ZSM-5 zeolite (MFI-type zeolite, Si/Al = 150 and 240) catalysts was examined at reaction temperatures ranging from 823 to 923 K under atmospheric pressure. The reaction rate constants and activation energies of *n*-hexane cracking over ZSM-5 zeolites with various crystal sizes and Si/Al ratios were evaluated. The catalytic cracking of *n*-hexane was first order with respect to the *n*-hexane concentration, and the activation energies of *n*-hexane cracking over ZSM-5 zeolites were found to be approximately 123-128 $kJmol^{-1}$. Compared with the macro-sized zeolite, the nano-sized zeolites exhibited high *n*-hexane conversion with stable activity for 50 h. This is because the cracking reaction with nano-sized zeolite proceeded under reaction-limiting conditions, whereas the reaction with macro-sized zeolite proceeded under transition conditions between reaction- and diffusion-limiting conditions. As a result, the application of nano-zeolite to the catalytic cracking of *n*-hexane was effective and gave light olefins with high yield and excellent stable activity.

Keywords

nano-zeolite, ZSM-5, naphtha, catalytic cracking, kinetic, Thiele modulus

1. Introduction

Light olefins are important basic raw materials for the petrochemical industry, and demand for light olefins such as ethylene and propylene is increasing every year [1, 2]. Light olefins have been mainly produced by thermal cracking of naphtha, which gives yields of ethylene and propylene of approximately 25% and 13%, respectively [3-5]. However, the naphtha cracking process is insufficient for the increased demand, because it is difficult to control the selectivity for specific light olefins. Moreover, because this process consumes more than 30% of the total amount of energy required in petrochemical refinement, developing efficient processes for the production of light olefins is indispensable. In comparison with thermal cracking, because the catalytic cracking of naphtha over solid-acid catalysts can achieve a high propylene/ethylene ratio at low reaction temperatures via the carbenium ion/β-scission mechanism [6, 7], using this process will reduce energy cost and provide selective production of propylene. Accordingly, the catalytic cracking of naphtha is expected to be an effective alternative to the thermal cracking process.

A promising catalyst for the catalytic cracking of naphtha is zeolite, which is a crystalline aluminosilicate material with various properties, such as strong acidity and high surface area, and studies on the catalytic cracking of alkane over zeolite catalysts have been reported [8-10]. Because zeolites possess intracrystalline micropores and nanospaces close to the molecular diameters of light hydrocarbons, they exhibit a remarkable molecular-sieving effect for light

hydrocarbons and have been widely used as shape-selective catalysts in various hydrocarbon processes (e.g., alkylation of aromatics [11, 12], as well as olefin synthesis from alcohol [13] and acetone [14, 15]). However, because the crystal sizes of zeolites are usually much larger than the sizes of the micropores, the rate-limiting step of the reaction tends to be the diffusion of the reactant/product molecules within the micropores. Moreover, carbon solid (coke) readily forms near the external surface of the crystal under diffusion-controlled conditions, thereby, rapidly plugging the pores, leading to a short catalyst lifetime. To achieve low diffusion resistance, nano-sized zeolites are effective because the diffusion length for reactant/product hydrocarbons, which depends on the zeolite crystal size, is reduced [16, 17].

We have successfully prepared MFI-type and MOR-type zeolite nanocrystals via hydrothermal synthesis in a water/surfactant/organic solvent (emulsion method) [18-22]. The nano-crystalline zeolites are expected to be promising materials with low diffusion resistance as well as a large external surface area, which improves the catalytic activity and lifetime. In the present study, selective synthesis for light olefins by the catalytic cracking of *n*-hexane over ZSM-5 zeolite (MFI-type zeolite) was carried out as a model reaction for the catalytic cracking of naphtha. The effect of crystal size of the zeolite on catalyst lifetime was investigated using the Thiele modulus and an effectiveness factor.

2. Experimental

2.1 Preparation of ZSM-5 zeolite with different crystal size

Nano-crystalline ZSM-5 zeolite (below 200nm) was prepared via hydrothermal synthesis using a water/surfactant/organic solvent (emulsion method) [19]. An aqueous solution containing a Si and Al source material was obtained by hydrolyzing each metal alkoxide in a dilute tetra-propyl-ammonium hydroxide (TPAOH)/water solution. The water solution (10 ml) thus obtained was added to the surfactant/organic solvent (70 ml, surfactant concentration of 0.5 mol/l). Poly-oxyethylene-(15)-oleylether and cyclohexane were employed as the surfactant and organic solvent, respectively. The water/surfactant/organic solvent thus obtained was poured into a Teflon-sealed stainless steel bottle and heated to 423 K for 72 h. In order to obtain macro-crystalline ZSM-5 zeolite (above 2000nm), hydrothermal synthesis was also carried out without the surfactant/organic solvent (conventional method). The precipitates thus obtained were washed with alcohol, dried at 373 K for 12 h, and calcined at 823 K for 3 h in an air stream. Physically adsorbed and/or ion-exchanged sodium ions on the zeolite surface were removed and exchanged with NH_4^+ by a conventional ion exchange technique with a 10% NH_4NO_3 aqueous solution, and then heated to 923 K to yield H-ZSM-5 zeolite. The powdered zeolite described above was pelletized, crushed and sieved to yield samples ca. 0.3 mm in diameter for the catalytic cracking reaction.

2.2 Characterization

The morphology and crystallinity of the obtained samples were analyzed by field emission scanning electron microscopy (FE-SEM; JSM-6500F, JEOL Co. Ltd.) and X-ray diffraction (XRD; JDX-8020, JEOL Co. Ltd.), respectively. The total and external surface areas of the obtained samples were calculated by BET- and *t*-methods, respectively, using an N_2 adsorption isotherm (Belsorp mini, BEL JAPAN Co. Ltd.). The Si/Al ratios of the samples were measured by X-ray fluorescence measurements (XRF; Supermini, Rigaku Co. Ltd.).

The acidity of the obtained samples (Si/Al = 150) were determined after adsorption of pyridine using FT-IR spectroscopy (FT/IR-4100, Jasco Co. Ltd.) [23, 24]. Because the analysis of high-silica zeolite encountered a difficulty due to a small amount of acid site, this procedure slightly differs from some preliminary experiments. The samples were activated in situ at 573 K for 1h before IR analysis. After cooling to room temperature, the reference spectrums of the activated samples were collected. The pyridine was adsorbed to the samples with the pyridine vapor pressure for 30 min at room temperature, followed by desorption of physically-adsorbed pyridine at room temperature for 20 min, and the spectrum was collected at room temperature. Additionally, the acidity of the obtained samples was also evaluated by the NH_3-TPD method [25]. In the TPD experiment, the carrier gas was 1.0% NH_3 (balance He), the heating rate was 5 K min^{-1}, and the temperature range was 373 - 823 K. The desorption of NH_3 molecules from the acid sites of the zeolite was measured under a 1.0% NH_3-He atmosphere so that the TPD profile

could be measured under complete adsorption equilibrium conditions, referred to as the *ac*-NH_3-TPD method.

2.3 Catalytic cracking of n-hexane over ZSM-5 zeolites

Catalytic cracking of *n*-hexane over ZSM-5 zeolite catalysts was carried out using a fixed-bed reactor at a reaction temperature of 823-923 K under N_2 at atmospheric pressure. A schematic of the reaction setup is shown in Fig. 1. The ZSM-5 zeolite catalyst was placed in a quartz tube reactor and activated in flowing N_2 at a reaction temperature for 1 h before each run. The quartz tube reactors with inner diameters of 4 and 10 mm were employed for the kinetic analysis and the investigation on the catalyst lifetime, respectively. *W/F* (*W*: amount of catalyst /g, *F*: feed rate /g h^{-1}) and the initial pressures of *n*-hexane as the feedstock were varied from 0.0072 to 0.125 h, and from 22.1 to 36.3 kPa, respectively. The composition of the exit gas was measured by on-line gas chromatography (GC-2014, Shimadzu Co. Ltd.) with a Porapak-Q column for the TCD detector and Gaskuropack-54 and SP-1700 columns for the FID detectors. The amount of coke deposited on the catalyst after reaction was measured by thermogravimetric analysis (TG; TGA-50, Shimadzu Co. Ltd.).

2.4 Measurement of n-Hexane Diffusivity within ZSM-5 Zeolites in the Vapor Phase

The intracrystalline diffusivity and amount of adsorbed *n*-hexane within ZSM-5 zeolites in the vapor phase were measured by the constant volumetric method [26-29]. The uptake curve of the amount adsorbed within the zeolite crystal can be expressed by the following theoretical equation for a zeolite crystal with a hexagonal slab shape.

$$\frac{M_t}{M_e} = 1 - \sum_{n=1} \frac{2\alpha(1+\alpha)}{1+\alpha+\alpha^2 q_n^2} \exp\left(-\frac{Dq_n^2 t}{L^2}\right) \qquad (1)$$

where $\alpha = V/(\alpha_m WHL)$, $\tan q_n = -\alpha q_n$ (2)

Here, M_t is the amount adsorbed at time t, M_e is the value of M_t at equilibrium, D is the intracrystalline diffusivity, L is the half-thickness value of the MFI-type zeolite crystal, a_m is the outer surface area of the zeolite crystal, W is the sample weight, V is the volume of the vapor phase, and H is the partition factor, which is the ratio of the concentration of adsorbed molecules within the catalyst to that in the gas phase. The effective diffusivity, D_{eff}, which is usually used for the kinetics analysis of the overall reaction rate by the Thiele modulus [30], is calculated by multiplying the intracrystalline diffusivity, D, with the partition factor, H. The details of the experimental apparatus and procedure are described in our previous papers [26-29].

3. Results and discussion

3.1 Preparation of ZSM-5 zeolites

Figure 2 shows the FE-SEM micrographs of the obtained zeolites with different crystal sizes and Si/Al ratios, respectively. Three different-sized ZSM-5 zeolites with different Si/Al ratios were obtained, and the crystal sizes were 2300 nm (Si/Al = 150), 150 nm (Si/Al = 150), 90 nm (Si/Al = 150), 2400 nm (Si/Al = 240) and 90 nm (Si/Al = 240), and denoted as MFI(*L*)150, MFI(*M*)150, MFI(*S*)150, MFI(*L*)240 and MFI(*S*)240, respectively. Figure 3 shows X-ray diffraction patterns of the samples obtained by the conventional and emulsion methods. The X-ray diffraction patterns of the samples showed peaks corresponding to the MFI-type zeolite. Figure 4 shows the NH_3-TPD profiles of the obtained zeolites with different crystal sizes and Si/Al ratios. Table 1 shows the Si/Al ratio measured by XRF and the total and external surface areas of the obtained samples. Since the Si/Al values measured by XRF were almost the same as each Si/Al ratio calculated from the Si and Al concentrations in the synthetic solution, it was considered that Al atoms in the synthetic solution were incorporated into the framework structures of the MFI-type zeolite during the hydrothermal synthesis. NH_3 desorption peaks at temperatures above 600 K were observed, which are associated with strong acid sites. Moreover, the area of the TPD profiles above 600 K depended on the Si/Al ratio of zeolites. While the external surface area increased with decreasing crystal size, the BET surface area of 400 m^2/g was almost constant regardless of the crystal size. Figure 5 shows the IR spectra of the MFI(*S*)150 and MFI(*L*)150 after adsorption of pyridine. Brønsted acid sites (1540 cm^{-1}) and Lewis acid sites (1460 cm^{-1}) were observed and the Brønsted acid / Lewis acid ratio was almost the same

(approximately 0.75) between MFI(*S*)150 and MFI(*L*)150. It is considered that the acidity of the obtained samples was not much difference regardless of crystal size. Accordingly, ZSM-5 zeolites with different crystal sizes and Si/Al ratios could be obtained and these zeolites could be used as catalysts for *n*-hexane cracking.

3.2 Reaction kinetics of n-hexane cracking

In order to evaluate the effects of crystal size and Si/Al ratio on the catalytic cracking of *n*-hexane in detail, the kinetics of the cracking reactions using ZSM-5 zeolites were investigated. In a differential reaction condition, the following relational expression is confirmed.

$$F_{A0} \triangle x_A / W = k_n \{C_{A0}(1 - \triangle x_A / 2)\}^n \qquad (3)$$

where F_{A0} is the molecular flux of *n*-hexane, $\triangle x_A$ is the conversion, W is the amount of catalyst, k_n is the reaction rate constant (differential reaction condition), C_{A0} is the initial concentration of *n*-hexane, and n is the reaction order. The relationship between $F_{A0} \triangle x_A$ and $C_{A0}(1-\triangle x_A / 2)$ obtained at 923 K is shown in Fig.7. From the relational expression, the slope of the plots in this figure represents a reaction order n. As shown in Fig. 7, because the slope of the plots was approximately 1.0 regardless of the crystal size and Si/Al ratio of the zeolite catalysts, it is considered that the catalytic cracking of *n*-hexane was first order with respect to the *n*-hexane concentration. The same dependency of the concentration on the reaction rate was observed at

the reaction temperature ranging from 823 to 923 K.

When the reaction is a first-order reaction under an integral reaction condition, the following relational expression can be applied;

$$W / F_{A0} = C_{A0} \int_0^{x_A} \frac{dx_A}{-r_A} = \frac{-\ln(1-x_A)}{kC_{A0}} \qquad (4)$$

where k is the reaction rate constant (integral reaction condition), and the relationship between W/F_{A0} and $-\ln(1-x_A)/C_{A0}$ obtained at 923 K is shown in Fig. 8. From the relational expression, the slope of the plots in this figure represents an inverse of the reaction rate constant $1/k$. As shown in Fig. 8, the reaction rate constants for the catalytic cracking of *n*-hexane at 923 K were 1.04×10^{-2}, 7.42×10^{-3} and 6.47×10^{-3} $m^3kg^{-1}s^{-1}$ with MFI(*S*)150, MFI(*S*)240 and MFI(*L*)240, respectively.

The reaction rate constants for the *n*-hexane cracking were obtained in accordance with the above-mentioned methods at reaction temperatures ranging from 823 to 923 K. Fig. 9 shows the Arrhenius plots for *n*-hexane cracking over ZSM-5 catalysts with different crystal sizes. The activation energies of the *n*-hexane cracking over ZSM-5 zeolites were found to be 126, 128 and 123 $kJmol^{-1}$ with MFI(*S*)150, MFI(*S*)240 and MFI(*L*)240, respectively. While MFI(*S*)150 and MFI(*S*)240 exhibited almost the same activation energy, MFI(*L*)240 showed a slightly smaller value compared with other catalysts. This is because the diffusivity of *n*-hexane within ZSM-5 zeolite with a large size affected the overall reaction rate constant, leading to a

decrease in the activation energy.

3.3 Effect of crystal size of ZSM-5 zeolite on the catalytic stability in n-hexane cracking

The effect of zeolite crystal size on the catalytic stability in *n*-hexane cracking was investigated using ZSM-5 zeolites (Si/Al = 150) with different crystal sizes. Changes in the *n*-hexane conversion and the product yields over ZSM-5 zeolites (Si/Al = 150) with different crystal sizes are shown in Fig. 10 and Table 2, respectively. Products including alkanes (methane, ethane, propane, and butanes), alkenes (ethylene, propylene, and butenes) and aromatics (benzene, toluene, and xylene (BTX)) were obtained; note that the amount of alkanes comprising C_5 and C_7^+ listed in Table 2 is denoted as others. In the case of thermal cracking, the *n*-hexane conversion was 15.0% under this reaction condition. The initial conversion of *n*-hexane was almost the same (approximately 94%) regardless of the crystal sizes, and the highest ethylene + propylene yield obtained was 53.5 C-mol% with a propylene/ethylene ratio of 1.57 at 94.1% conversion over MFI(*S*)150. However, the conversion gradually decreased with time on stream over MFI(*L*)150, decreasing to 48% after 50 h. In contrast, MFI(*S*)150 and MFI(*M*)150 maintained high conversions at 82 and 81%, respectively, after 50 h, and were hardly changed from the start of reaction. Moreover, the stable activity of the nano-zeolites (MFI(*S*)150 and MFI(*M*)150) gave stable product selectivities compared with the macro-zeolite (MFI(*L*)150).

It is believed that coke formation resulted in the deactivation of zeolite catalysts. Therefore, the amounts of coke deposited on the zeolites after the reaction for 50 h were measured (Table 2). Moreover, N_2 adsorption isotherms of these zeolites before/after the reaction are shown in Figs. 11. The amount of coke formed after the reaction (50 h) increased with decreasing crystal size. Compared with the macro-zeolite (MFI(*L*)150), the N_2 adsorption isotherms of nano-zeolites (MFI(*S*)150 and MFI(*M*)150) were nearly unchanged after the cracking reaction even though a large amount of coke was deposited on the nano-zeolites. Accordingly, it is considered that the coke formation mainly occurred on the external surface of the zeolite crystals. In the macro-zeolite, since the external surface area was small, the pore plugging deeply occurred by the coke deposition, and thus the catalytic activity decreased. On the other hand, the nano-zeolites with a large external surface area suffered much less deactivation by coke deposition than the macro-zeolite. Accordingly, it was found that the crystal size of zeolite significantly reduced the catalytic activity, and that application of the nano-zeolite to *n*-hexane cracking was effective in the stabilization of the catalytic activity.

3.4 Effectiveness factor for n-hexane cracking over ZSM-5 zeolites with different crystal sizes

To investigate the effect of crystal sizes on the catalyst activity in detail, the Thiele modulus and the effectiveness factor for *n*-hexane cracking were calculated using the reaction rate constant and the effective diffusivity. The intracrystalline diffusivity of

n-hexane within the MFI-type zeolites in the vapor phase was measured by the constant volumetric method [26-29]. Because the thermal and catalytic cracking of *n*-hexane occurs at temperatures above 673 K, the effective diffusivity of n-hexane was measured using silicalite-1 (MFI-type zeolite without Al). The effective diffusivity, D_{eff}, under the catalytic cracking condition was estimated to be 1.30 $\times 10^{-11}$ $\mathrm{m^2 s^{-1}}$ using the obtained value below 573 K.

The relationship between the Thiele modulus, ϕ, and the effectiveness factors, η, was calculated according to the following equation.

$$\phi = \frac{V}{S}\sqrt{\frac{k \times \rho_{\mathrm{p}}}{D_{\mathrm{eff}}}} = L\sqrt{\frac{k \times \rho_{\mathrm{p}}}{D_{\mathrm{eff}}}}, \quad V = \frac{1}{2}S \times 2L \quad \text{in a slab-shape crystal} \qquad (5)$$

$$\eta = \frac{\tanh(\phi)}{\phi} \qquad (6)$$

where V is the volume of the zeolite crystal, S is the external surface area of the zeolite crystal, L is the half-thickness value of the MFI-type zeolite crystal, and ρ_{p} is the density of the zeolite crystal. The Thiele modulus and the effectiveness factors for the reaction using ZSM-5 zeolites with different crystal sizes were calculated, and the results are shown in Fig. 12 and Table 3. The effectiveness factor of MFI(*S*)150 was 1.0, indicating that the catalytic reaction in MFI(*S*)150 proceeded under reaction-controlling conditions.

Because it was revealed that the cracking reaction proceeded under the reaction-limiting conditions in MFI(*S*)150, the reaction rate constant was applied to evaluate the Thiele modulus for the other zeolites (MFI(*M*)150 and MFI(*L*)150) using equation (5). The

crystal sizes of MFI(*M*)150 and MFI(*L*)150 were substituted into equation (5), and the effectiveness factors for these zeolites were calculated to be 1.0 and 0.65, respectively. While the catalytic cracking reaction with MFI(*M*)150 proceeded under reaction-controlling conditions along with MFI(*S*)150, the reaction with MFI(*L*)150 proceeded under transition conditions. Accordingly, it was considered that MFI(*L*)150 differed from the other catalysts in the *n*-hexane conversion with time on stream, as shown in Fig. 10. When the Thiele modulus, ϕ, is less than 0.1, the reaction proceeds under reaction-limiting conditions. By substituting a ϕ of 0.1 into equation (5), the crystal size of zeolite required to achieve reaction-limiting conditions can be obtained. It is revealed that ZSM-5 zeolite (Si/Al = 150) with a crystal size below 170 nm is required for *n*-hexane cracking under reaction-limiting conditions. This result was in good agreement with the changes in the *n*-hexane conversion with time on stream, using MFI(*S*)150 and MFI(*M*)150, as shown in Fig. 10.

Additionally, the reaction rate constants for the coked samples after the reaction (50 h) were obtained in the same manner as discussed in section 3.2 (Table 3). The reaction rate constants were 8.27 $\times 10^{-3}$ and 4.24 $\times 10^{-3}$ $m^3kg^{-1}s^{-1}$, for coked MFI(*S*)150 and coked MFI(*L*)150, respectively. The effectiveness factors for these coked zeolites were calculated as the ratios of the reaction rate constants of the coked zeolites to that of MFI(*S*)150 at the initial reaction time, as listed in Table 3. Because the Thiele modulus of the macro-zeolite (MFI(*L*)150) at the initial reaction time had a high value of above 1.0, the effectiveness factor

gradually decreased from 0.65 to 0.41 during the reaction. On the other hand, since the Thiele modulus of the nano-zeolite (MFI(*S*)150) at the initial reaction time had a low value of less than 0.1, only a slight change in the high effectiveness factor of 0.80 was observed after a reaction time of 50 h. The decrease in the effectiveness factor resulted from coke deposition during the cracking reaction. The large external surface area and low diffusion resistance of the macro-zeolite could limit the effect of coke deposition on the reduced catalytic activity.

4. *Conclusion*

Catalytic cracking of *n*-hexane over ZSM-5 zeolite catalysts was examined at a reaction temperature of 823-923 K under atmospheric pressure. The reaction rate constant and the activation energies of *n*-hexane cracking over ZSM-5 zeolites with different crystal sizes and Si/Al ratios were evaluated. Compared with the macro-zeolite, the nano-zeolites exhibited high *n*-hexane conversion with stable activity for 50 h. This is because the cracking reaction with the nano-zeolites proceeded under reaction-limiting conditions, whereas the reaction with the macro-zeolite proceeded under transition conditions. Moreover, the large external surface area and low diffusion resistance of the nano-zeolites reduce the effect of pore plugging due to coke deposition. As a result, the application of nano-zeolite in the catalytic cracking of *n*-hexane was effective in the stabilization of the catalytic activity.

Acknowledgement

This work was supported by a Research Grant Program of the New Energy and Industrial Technology Development Organization (NEDO) of Japan and the Global COE Program (Project No. B01: Catalysis as the Basis for Innovation in Materials Science) from the Ministry of Education, Culture, Sports, Science and Technology, Japan.

References

[1] O. Bortnovsky, P. Sazama, B. Wichterlova, Cracking of pentenes to C_2–C_4 light olefins over zeolites and zeotypes: Role of topology and acid site strength and concentration, *Appl. Catal. A Gen.*, 287 (2005) 203-213

[2] C. Mei, P. Wen, Z. Liu, Y. Wang, W. Yang, Z. Xie, W. Hua, Z. Gao, Selective production of propylene from methanol: Mesoporosity development in high silica HZSM-5, *J. Catal.*, 258 (2008) 243-249

[3] J. S. Jung, J. W. Park, G. Seo, Catalytic cracking of n-octane over alkali-treated MFI zeolites, *Appl. Catal. A Gen.*, 288 (2005) 149-157

[4] T. Komatsu, H. Ishihara, Y. Fukui, T. Yashima, Selective formation of alkenes through the cracking of n-heptane on Ca^{2+}-exchanged ferrierite, *Appl. Catal. A Gen.*, 214 (2001) 103-109

[5] J. S. Plotkin, The changing dynamics of olefin supply/demand, *Catal. Today*, 106 (2005) 10-14

[6] Y. Yoshimura, N. Kijima, T. Hayakawa, K. Murata, K. Suzuki, F. Mizukami, K. Matano, T. Konishi, T. Oikawa, M. Saito, T. Shiojima, K. Shiozawa, K. Wakui, G. Sawada, K. Sato, S. Matsuo, N. Yamaoka, Catalytic cracking of naphtha to light olefins, *Catal. Surv. Jpn.*, 4 (2000) 157-167

[7] A. Corma , A.V. Orchillès, *Micropor. Mesopor. Mater.*, Current views on the mechanism of catalytic cracking, 35 (2000) 21-30

[8] P. Magnoux, P. Cartraud, S. Mignard, M. Guisnet, Coking, aging, and regeneration of zeolites: III. Comparison of the deactivation modes of H-mordenite, HZSM-5, and HY during n-Heptane cracking. *J. Catal.*, 106 (1987) 242-250

[9] A. Corma , V. Gonzàlez-Alfaro, A.V. Orchillès, Catalytic cracking of alkanes on MCM-22 zeolite. Comparison with ZSM-5 and beta zeolite and its possibility as an FCC cracking additive, *Appl. Catal. A Gen*., 129 (1995) 203-215

[10] N. Katada, Y. Kageyama, K. Takahara, T. Kanai, H.A. Beguma, M. Niwa, Acidic property of modified ultra stable Y zeolite: increase in catalytic activity for alkane cracking by treatment with ethylenediaminetetraacetic acid salt, *Catal., A Chem.* 211 (2004) 119-130

[11] Y. Sugi, Y. Kubota, K. Komura, N. Sugiyama, M. Hayashi, J. H. Kim, G. Seo, Shape-selective alkylation and related reactions of mononuclear aromatic hydrocarbons over H-ZSM-5 zeolites modified with lanthanum and cerium oxides, *Appl. Catal. A Gen*., 299 (2006) 157-166

[12] S. Inagaki, K. Kamino, E. Kikuchi, M. Matsukata, Shape selectivity of MWW-type aluminosilicate zeolites in the alkylation of toluene with methanol, *Appl. Catal. A Gen*., 318 (2007) 22-27

[13] T. Tago, K. Iwakai, K. Morita, K. Tanaka, T. Masuda, Control of acid-site location of ZSM-5 zeolite membrane and its application to the MTO reaction, *Catal. Today,* 105 (2005) 662-666

[14] T. Tago, H. Konno, S. Ikeda, S. Yamazaki, W. Ninomiya, Y. Nakasaka, T. Masuda, Selective production of isobutylene from acetone over alkali metal ion-exchanged BEA zeolites, *Catal. Today*, 164 (2011) 158-162

[15] T. Tago, H. Konno, M. Sakamoto, T. Masuda, Selective synthesis for light olefins from acetone over ZSM-5 zeolites with nano- and macro-crystal sizes, *Appl. Catal. A Gen.*, 403 (2011) 183-191

[16] H. Mochizuki, T. Yokoi, H. Imai, R. Watanabe, S. Namba, J. N. Kondo, T. Tatsumi, Facile control of crystallite size of ZSM-5 catalyst for cracking of hexane, *Micropor. Mesopor. Mater.*, 145 (2011)165-171

[17] H. Konno, T. Okamura, Y. Nakasaka, T. Tago, T. Masuda, Effects of crystal size and Si/Al ratio of MFI-type zeolite catalyst on *n*-hexane cracking for light olefin synthesis, *J. Jpn. Petrol. Inst.*, 55 (2012) 267-274

[18] T. Tago, M. Nishi, Y. Kouno, T. Masuda, New Method for Preparing Mono-Dispersed Nano-Crystalline Silicalite via Hydrothermal Synthesis in Water/Surfactant/Oil Solution, *Chem. Lett.*, 33 (2004) 1040-1041

[19] T. Tago, K. Iwakai, M. Nishi, T. Masuda, Synthesis of Mono-Dispersed Silicalite-1 Nanocrystals in Water-Surfactant-Organic Solvent, *J. Nanosci. Nanotechnol.*, 9 (2009) 612-617

[20] T. Tago, D. Aoki, K. Iwakai, T. Masuda, Preparation for Size-Controlled MOR Zeolite Nanocrystal Using Water/Surfactant/Organic Solvent, *Top. Catal*., 52 (2009) 865-871

[21] T. Tago, M. Sakamoto, K. Iwakai, H. Nishihara, S.R. Mukai, T. Tanaka, T. Masuda, Control of Acid-Site Location of MFI Zeolite by Catalytic Cracking of Silane and its Application to Olefin Synthesis from Acetone, *J. Chem. Eng. Jpn*., 42 (2009) 162-167

[22] K. Iwakai, T. Tago, H. Konno, Y. Nakasaka, T. Masuda, Preparation of nano-crystalline MFI zeolite via hydrothermal synthesis in water/surfactant/organic solvent using fumed silica as the Si source, *Micropor. Mesopor. Mater.*, 141 (2011) 167-174

[23] E. P. Parry, An Infrared Study of Pyridine Adsorbed on Acidic Solids. Characterization of Surface Acidity, *J. Catal.*, 2 (1963) 371-379

[24] Zuzana Musilova-Pavlackova, Stacey I. Zones, Jiri Cejka, Post-Synthesis Modification of SSZ-35 Zeolite to Enhance the Selectivity in *p*-Xylene Alkylation with Isopropyl Alcohol, *Top. Catal.*, 53 (2010) 273-282

[25] T. Tago, Y. Okubo, S. R. Mukai, T. Tanaka, T. Masuda, Simultaneous characterization of acidic and basic properties of solid catalysts by a new TPD method and their correlation to reaction rates, *Appl. Catal. A Gen*., 290 (2005) 54-64

[26] T. Masuda, Diffusion Mechanisms of Zeolite Catalysts, *Catal. Surv. Asia*, 7 (2003) 133-144

[27] T. Masuda, K, Fukada, Y. Fujikata, H. Ikeda, K. Hashimoto, Measurement and prediction

of the diffusivity of Y-type zeolite. *Chem. Eng. Sci.*, 51 (1996) 1879-1888.

[28] T. Masuda, Y. Okubo, S. R. Mukai, M. Kawase, K. Hashimoto, A. Shichi, A. Satsuma, T. Hattori, Y. Kiyozumi, Effective diffusivities of lighter hydrocarbons in Cu- and Co-MFI-type zeolite catalysts. *Chem. Eng. Sci.*, 56 (2001) 889-896.

[29] T. Masuda, Y. Fujikata, T. Nishida, K. Hashimoto, The influence of acid sites on intracrystalline diffusivities within MFI-type zeolites, *Micropor. Mesopor. Mater.*, 23 (1998) 157-167

[30] E. W. Thiele, Relation between Catalytic Activity and Size of Particle, *Ind. Eng. Chem.*, 31 (1939) 916-920

Figure and Table captions

Fig. 1. Experimental setup of the fixed-bed flow reactor.

Figs. 2. SEM micrographs of ZSM-5 zeolites with different crystal sizes and Si/Al ratios.

Fig. 3. XRD patterns of ZSM-5 zeolites with different crystal sizes and Si/Al ratios.

Fig. 4. NH_3-TPD profiles of ZSM-5 zeolites with different crystal sizes and Si/Al ratios.

Fig. 5. IR spectra (a) MFI(*S*)150 and (b) MFI(*L*)150 after adsorption of pyridine.

Fig. 6. Relationship between $F_{A0}\triangle x_A/W$ and $C_{A0}(1-\triangle x_A/2)$ in *n*-hexane cracking over ZSM-5 zeolites. Reaction conditions: T = 923 K, W/F = 0.0072-0.0174 h, P = 22.1-36.3 kPa.

Fig. 7. Relationship between W/F_{A0} and $-\ln(1-x_A)/C_{A0}$ in *n*-hexane cracking over ZSM-5 zeolites. Reaction conditions: T = 923 K, W/F = 0.0072-0.0174 h, P = 22.1-36.3 kPa.

Fig. 8. Arrhenius plot of *n*-hexane cracking over ZSM-5 zeolites. Reaction conditions: T = 823-923 K, W/F = 0.0072-0.0174 h, P = 22.1-36.3 kPa.

Fig. 9. *n*-Hexane conversion over time in *n*-hexane cracking over ZSM-5 zeolite (Si/Al = 150) with different crystal sizes. Reaction conditions: T = 923 K, W/F = 0.125 h, P = 22.1 kPa.

Figs. 10. N_2 adsorption isotherms of ZSM-5 zeolites with different crystal sizes before/after the *n*-hexane cracking reaction (50 h). (a) MFI(*S*)150, (b) MFI(*M*)150, (c) MFI(*L*)150.

Fig. 11. Relationship between the Thiele modulus and the effectiveness factor in *n*-hexane cracking at 923 K over ZSM-5 zeolites (Si/Al = 150) with different crystal sizes.

Table 1. BET and external surface areas of ZSM-5 zeolites with different crystal sizes and Si/Al ratios. S_{BET}: surface area by the BET method, S_{ext}: external surface area by the *t*-method.

Table 2. *n*-Hexane conversion, product yields and coke amounts over MFI(*S*)150, MFI(*M*)150 and MFI(*L*)150.

Table 3. Effectiveness factors of ZSM-5 zeolites (Si/Al = 150) with different crystal sizes in *n*-hexane cracking at 923 K.

Fig. 1. Experimental setup of the fixed-bed flow reactor.

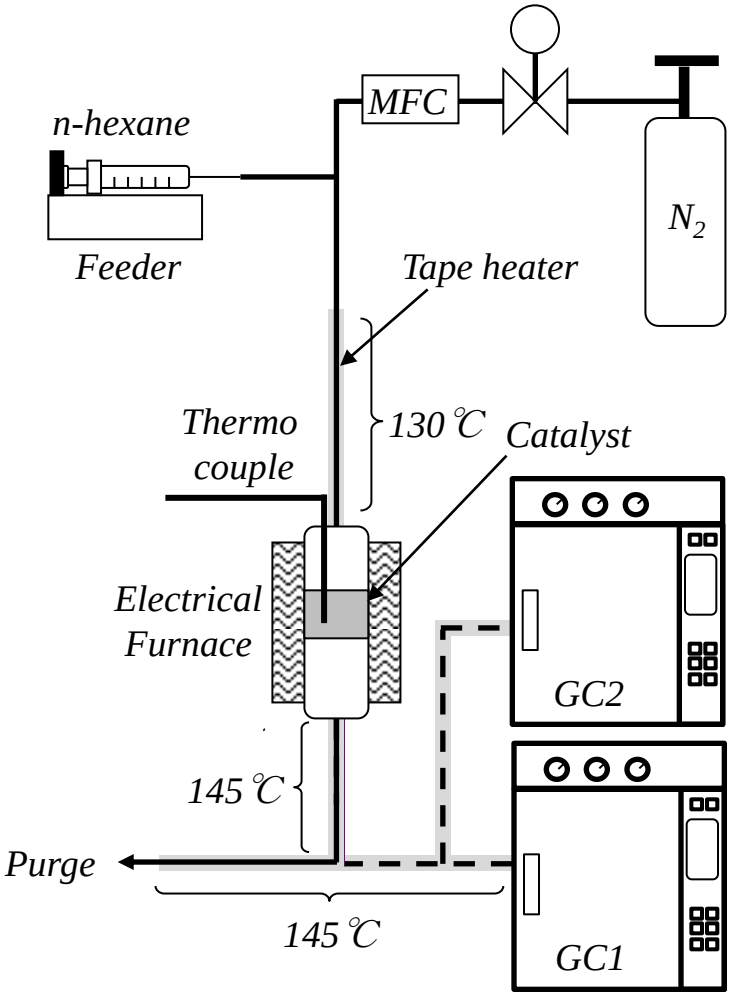

Figs. 2. SEM micrographs of ZSM-5 zeolites with different crystal sizes and Si/Al ratios.

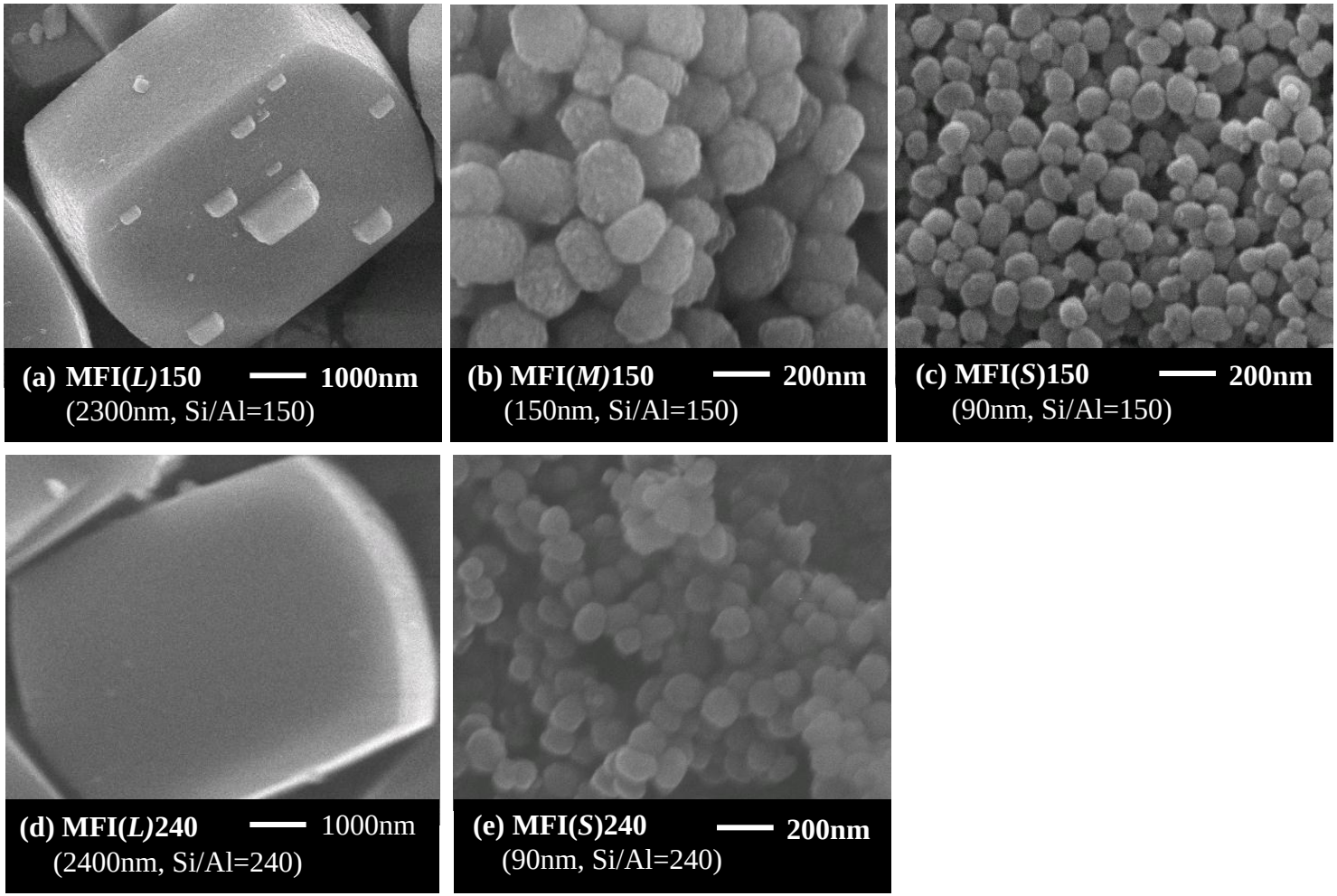

Fig. 3. XRD patterns of ZSM-5 zeolites with different crystal sizes and Si/Al ratios.

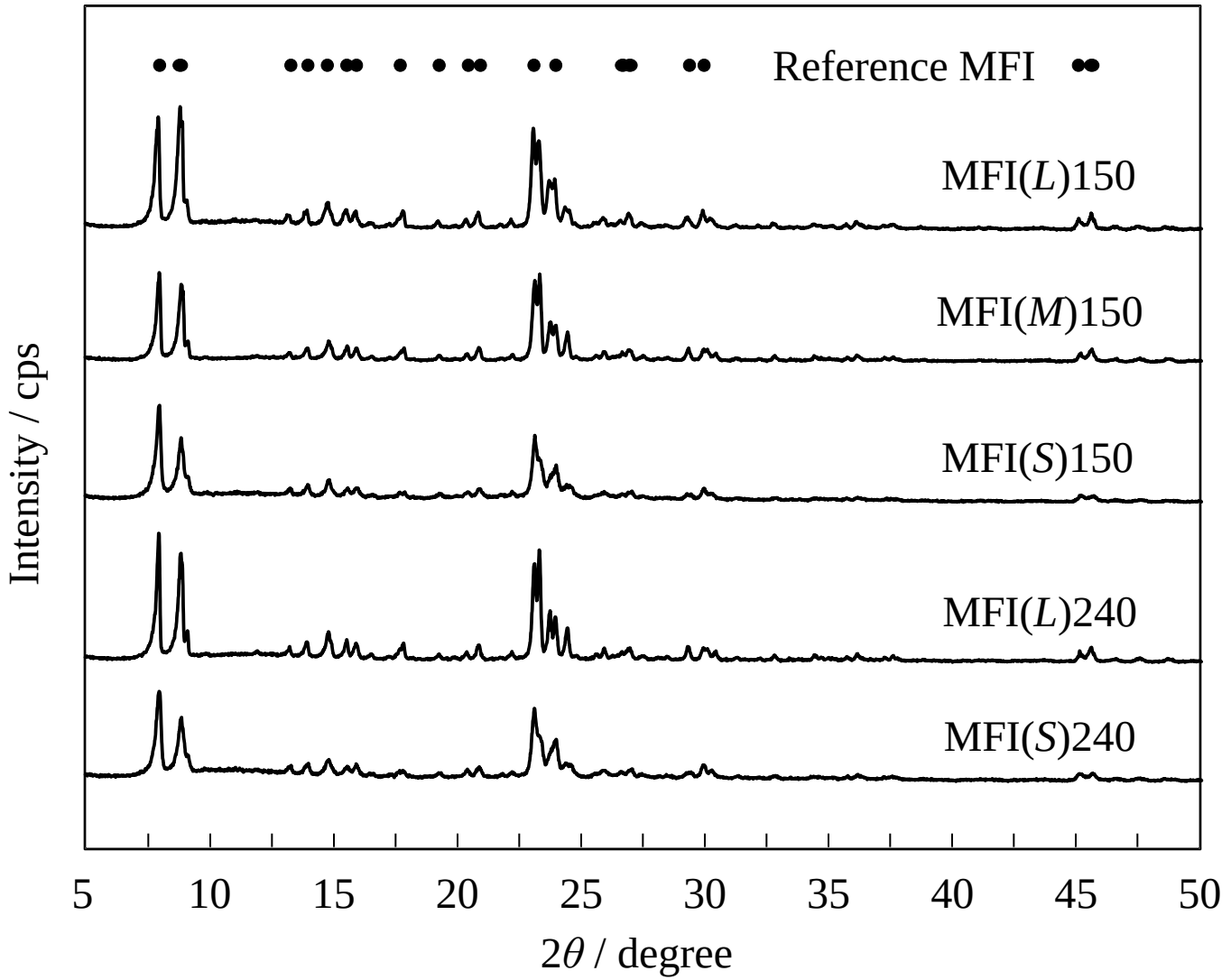

Fig. 4. NH_3-TPD profiles of ZSM-5 zeolites with different crystal sizes and Si/Al ratios.

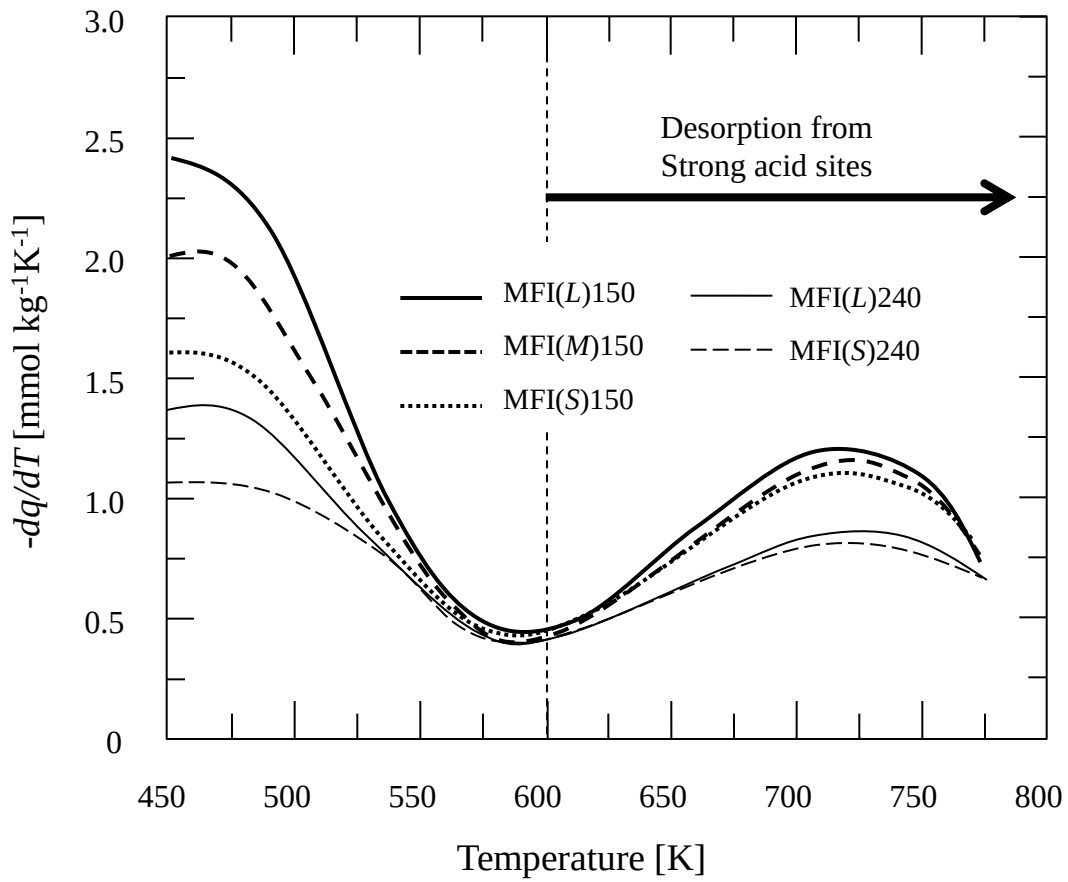

Fig. 5. IR spectra (a) MFI(*S*)150 and (b) MFI(*L*)150 after adsorption of pyridine.

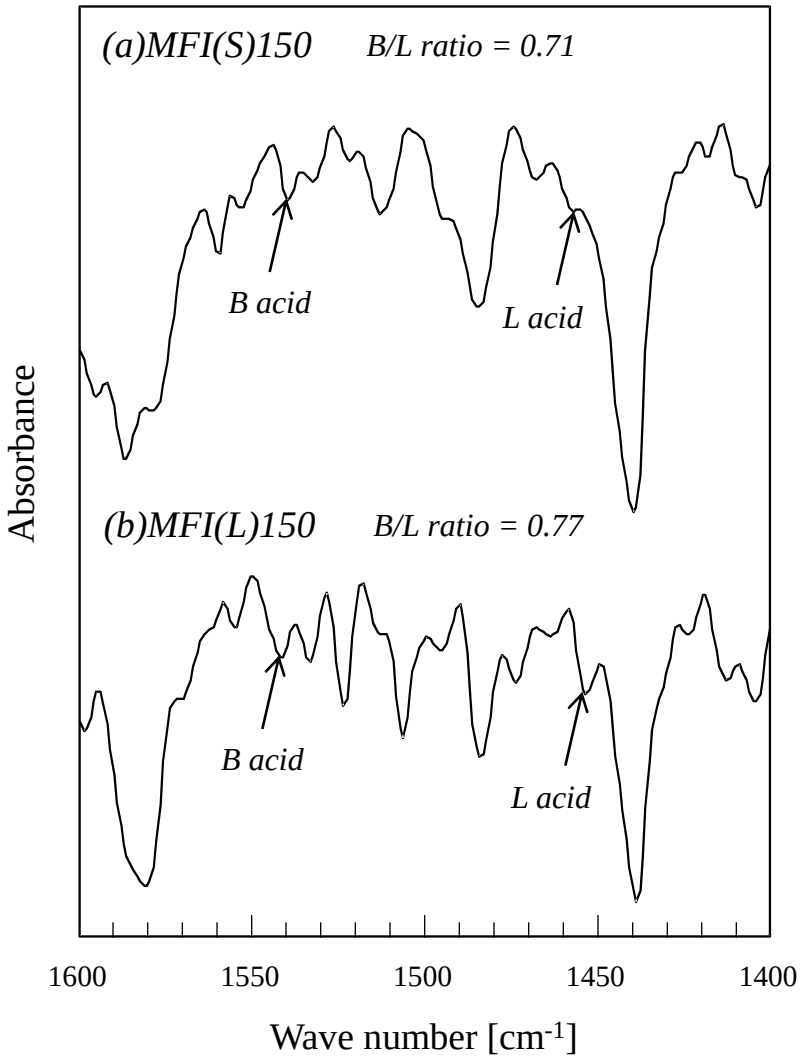

Fig. 6. Relationship between $F_{A0}\triangle x_A/W$ and $C_{A0}(1-\triangle x_A/2)$ in the *n*-hexane cracking over ZSM-5 zeolites. Reaction conditions: T = 923K, W/F = 0.0072-0.0174h, P = 22.1-36.3 kPa.

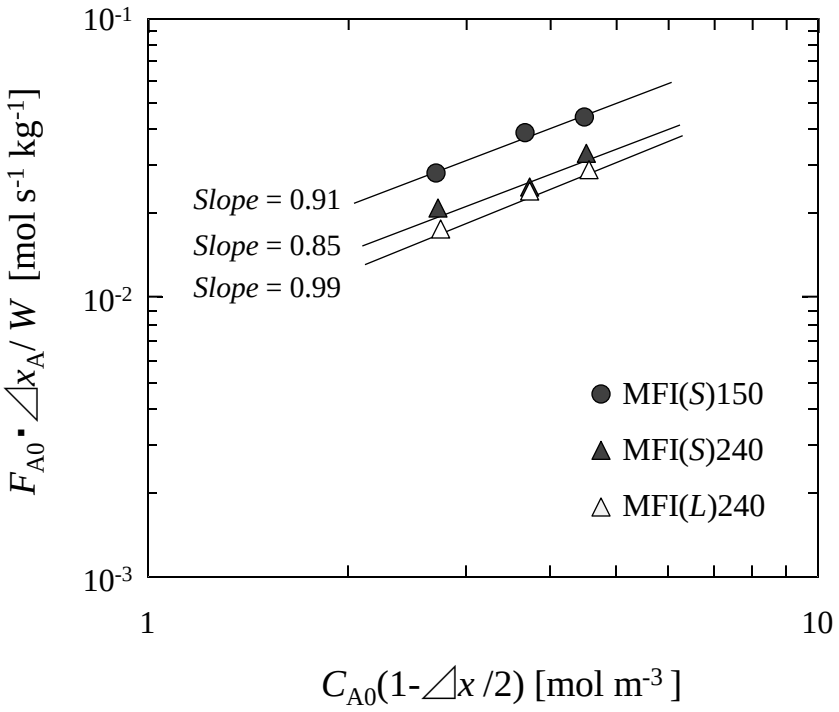

Fig. 7. Relationship between W/F_{A0} and $-\ln(1-x_A)/C_{A0}$ in the *n*-hexane cracking over ZSM-5 zeolites. Reaction conditions: T = 923K, W/F = 0.0072-0.0174h, P = 22.1-36.3 kPa.

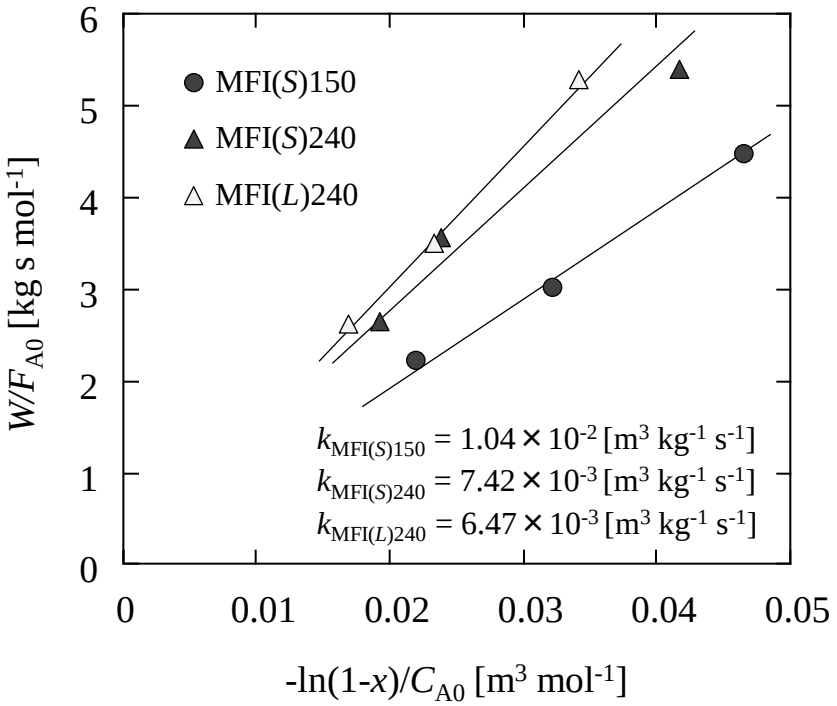

Fig. 8. Arrhenius plot of *n*-hexane cracking over ZSM-5 zeolites.
Reaction conditions: T = 823-923K, W/F = 0.0072-0.0174h, P = 22.1-36.3 kPa.

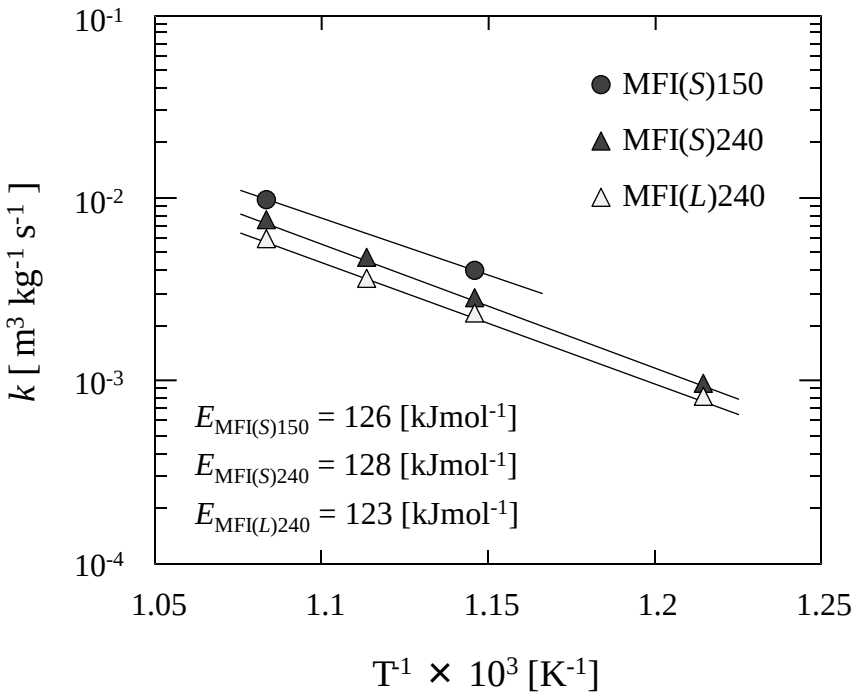

Fig. 9. *n*-Hexane conversion over time in *n*-hexane cracking reaction over the ZSM-5 zeolite (Si/Al=150) with different crystal sizes. Reaction conditions: T = 923K, W/F = 0.125h, P = 22.1kPa.

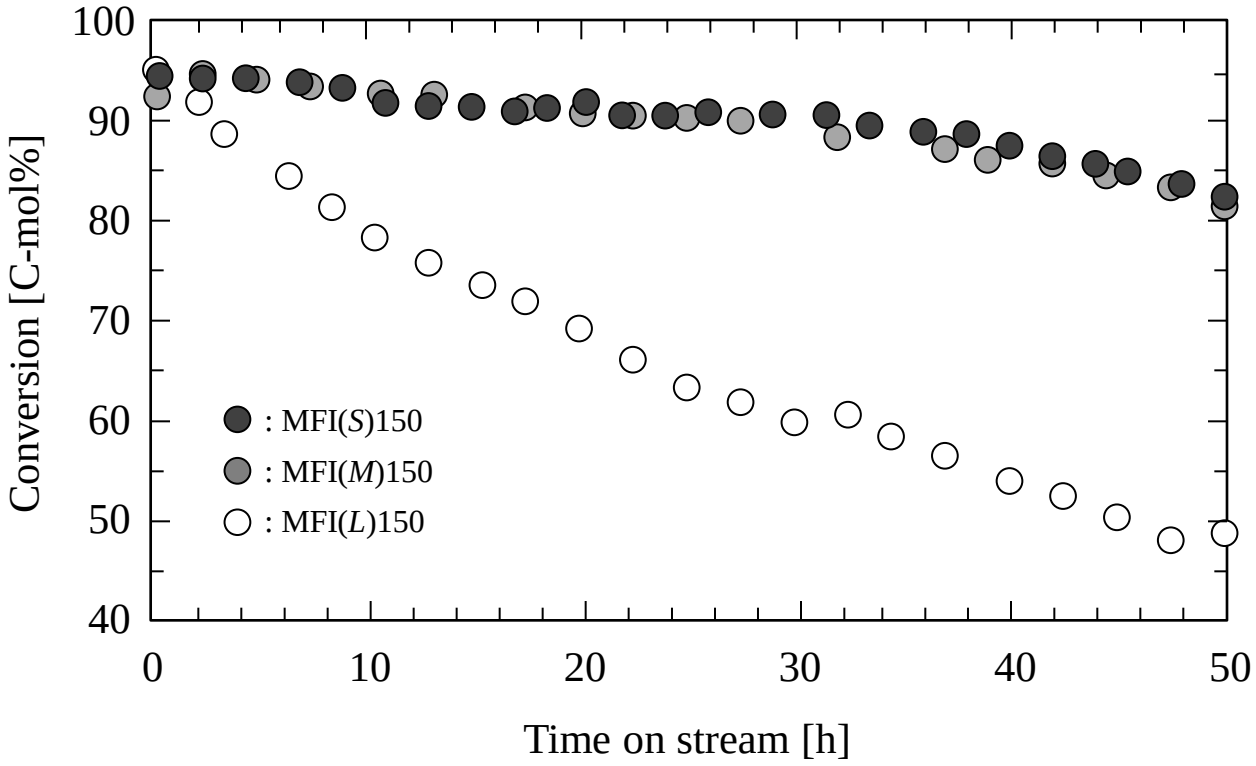

Figs. 10. N_2 adsorption isotherms of ZSM-5 zeolites with different crystal sizes before/after the *n*-hexane cracking reaction (50h). (a) MFI(*S*)150, (b) MFI(*M*)150 and (c) MFI(*L*)150.

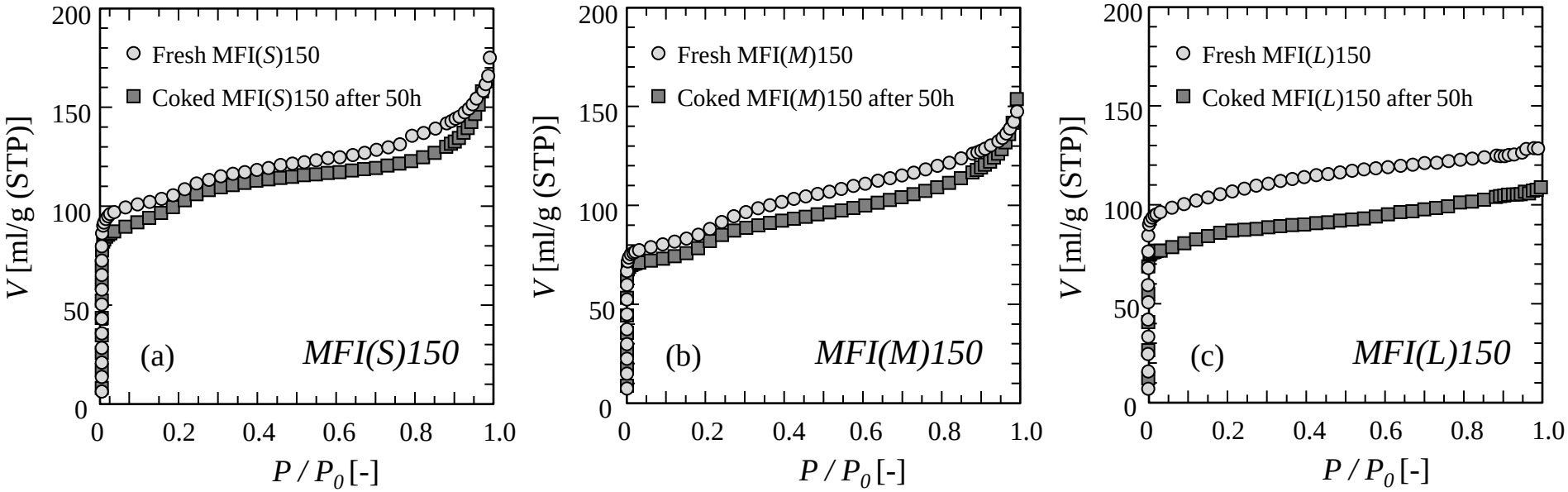

Fig. 11. Relationship between the Thiele modulus and effectiveness factor in the *n*-hexane cracking at 923K over ZSM-5 zeolites (Si/Al = 150) with different crystal sizes.

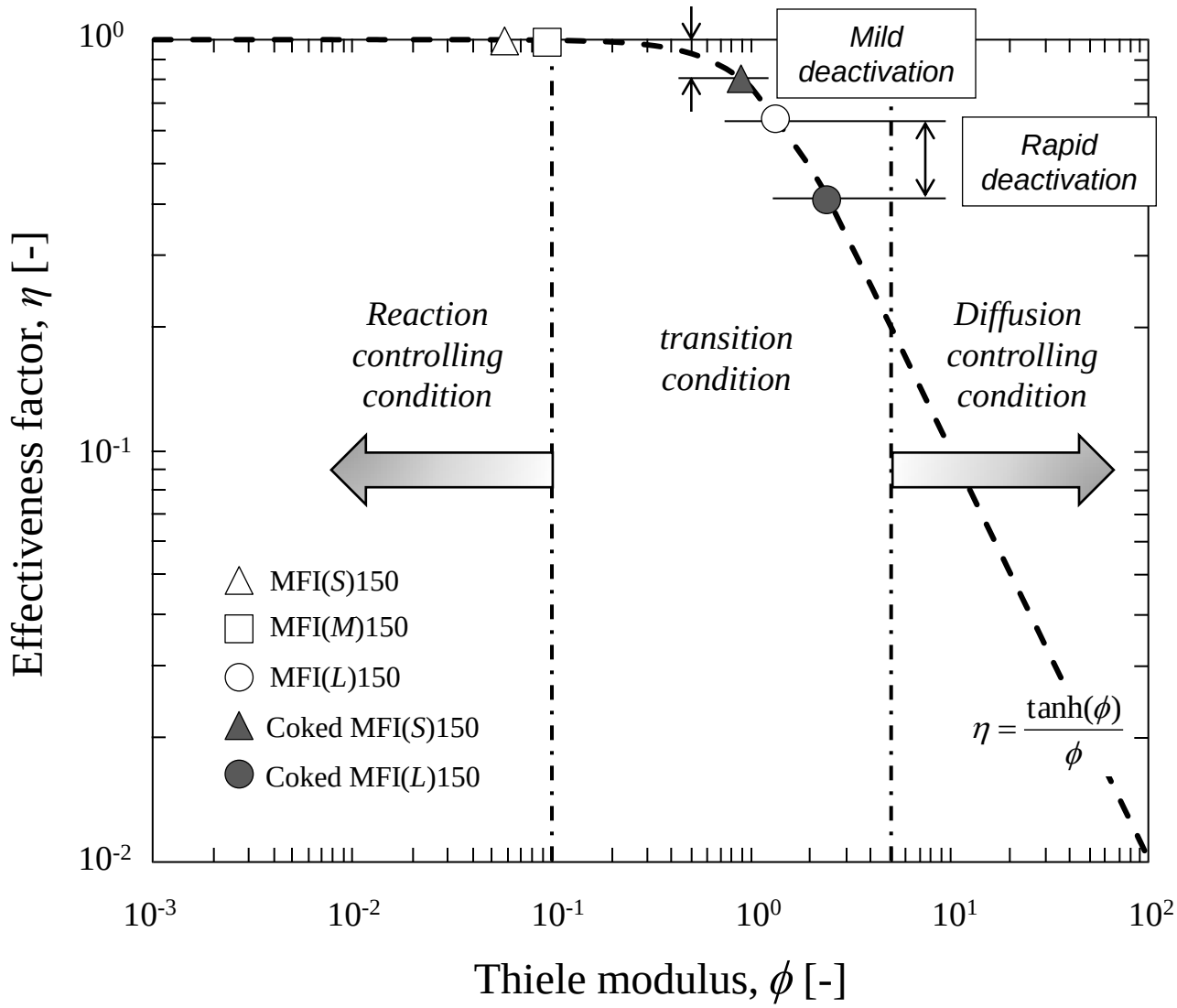

Table 1. BET and external surface areas of ZSM-5 zeolites with different crystal size and Si/Al ratio. S_{BET}: surface area by BET method, S_{ext}: external surface area by *t*-method.

Sample	S_{BET}[$m^2 g^{-1}$]	S_{ext}[$m^2 g^{-1}$]	Si/Al measured by XRF
MFI(*S*)150	397	42.8	192
MFI(*M*)150	365	33.8	180
MFI(*L*)150	402	5.9	158
MFI(*S*)240	409	44.4	320
MFI(*L*)240	410	4.3	290

Table 2. *n*-Hexane conversion, product yields and coke amounts over MFI(*S*)150, MFI(*M*)150 and MFI(*L*)150.

Catalyst	Time [h]	Conversion [C-mol%]	Light olefins yield [C-mol%]				BTX yield [C-mol%]	Others yield [C-mol%]	Coke amount of after 50h [wt%]
			$C_2^=$	$C_3^=$	$C_4^=$	Total olefins			
MFI(*S*)150	0.50	94.1	20.8	32.7	3.8	57.3	4.2	32.6	-
	7.00	93.5	19.1	32.8	4.0	55.9	4.1	33.5	-
	50.0	82.0	13.2	29.0	4.7	46.9	4.5	30.6	59.6
MFI(*M*)150	0.33	92.2	22.8	30.3	6.6	59.7	4.3	28.2	-
	7.50	93.1	20.8	32.4	7.3	60.5	3.9	28.7	-
	50.0	81.0	13.6	31.3	8.4	53.3	2.6	25.1	21.0
MFI(*L*)150	0.33	94.7	23.9	28.6	5.9	58.4	6.2	30.1	-
	8.50	81.0	13.6	30.8	8.1	52.5	3.1	25.4	-
	50.0	48.3	6.2	19.5	6.3	32.0	1.5	14.8	7.5

Table 3. Effectiveness factors of ZSM-5 zeolites (Si/Al = 150) with different crystal sizes in *n*-hexane cracking at 923K.

Sample	Reaction rate constant k [$m^3\ kg^{-1}\ s^{-1}$]	Thiele modulus ϕ [-]	Effectiveness factor η [-]
MFI(*S*)150	1.04×10^{-2}	5.38×10^{-2}	1.00
MFI(*M*)150	-	8.97×10^{-2} *	1.00
MFI(*L*)150	-	1.38 *	0.65
Coked MFI(*S*)150	8.27×10^{-3}	9.03×10^{-1}	0.80
Coked MFI(*L*)150	4.24×10^{-3}	2.41	0.41

* : theoretical value calculated from reaction rate constant of MFI(*S*)150